Published in final edited form as:
Histochem Cell Biol. 2009 April ; 131(4): 471–481. doi:10.1007/s00418-008-0541-5.

Characterization of the Inflammatory and Fibrotic Response in a Mouse Model of Cardiac Pressure Overload

Xia Ying, **Keunsang Lee**, **Na Li**, **Daniel Corbett**, **Leonardo Mendoza**, and **Nikolaos G Frangogiannis**
Section of Cardiovascular Sciences, Department of Medicine, Baylor College of Medicine, Houston, TX

Abstract

Myocardial fibrosis is an integral component of most cardiac pathologic conditions and contributes to the development of both systolic and diastolic dysfunction. Because of the availability of genetically manipulated animals, mouse models are essential for understanding the mechanisms involved in the pathogenesis of cardiac fibrosis. Accordingly, we characterized the inflammatory and fibrotic response in a mouse model of cardiac pressure overload due to transverse aortic constriction (TAC). Following TAC, mouse hearts exhibited induction of chemokines and proinflammatory cytokines, associated with macrophage, but not neutrophil, infiltration. Induction of inflammatory cytokines was followed by a late upregulation of Transforming Growth Factor (TGF)-β isoforms, activation of the Smad2/3 and Smad1/5 pathways, induction of matricellular proteins, and deposition of collagen. Inflammatory activity decreased after 28 days of TAC; at this timepoint established fibrosis was noted, accompanied by ventricular dilation and systolic dysfunction. Late induction of inhibitory mediators, such as TGF-β may play an essential role in the transition from inflammation to fibrosis by suppressing inflammatory gene synthesis while inducing matrix deposition. Our findings identify molecular mediators and pathways with a potential role in cardiac fibrosis laying the foundations for studies exploring the pathogenesis of fibrotic cardiac remodeling using genetically targeted mice.

Keywords

cytokine; chemokine; TGF-β; cardiac fibrosis; inflammation

Introduction

Myocardial fibrosis is an integral component of most cardiac pathologic conditions (Brown et al. 2005). Accumulation of extracellular matrix in the cardiac interstitium disrupts the coordination of myocardial excitation-contraction coupling in both systole and diastole and may result in profound functional impairment (Janicki and Brower 2002). Beyond its effects on function, myocardial fibrosis also promotes arrhythmogenesis through impaired anisotropic conduction and subsequent generation of reentry circuits (Khan and Sheppard 2006).

Because the heart has negligible regenerative capacity, most forms of cardiac injury ultimately result in the development of fibrosis. Myocardial infarction is associated with death of a large number of cardiomyocytes and sets into motion a reparative response leading to formation of a collagen-based scar (Cleutjens et al. 1995). Extensive evidence suggests the involvement of

Address for correspondence: Nikolaos G. Frangogiannis, MD, Section of Cardiovascular Sciences, One Baylor Plaza M/S BCM620, Baylor College of Medicine, Houston, TX 77030, Tel: 713-798-4188, Fax: 713-796-0015, ngf@bcm.tmc.edu.

inflammatory mechanisms in post-infarction cardiac repair (Frangogiannis 2006b). Cardiomyocyte death triggers an acute inflammatory reaction resulting in infiltration of the infarcted myocardium with leukocytes that clear the wound from dead cells and matrix debris. Subsequent activation of inhibitory mediators, such as TGF-β, suppresses proinflammatory gene synthesis while promoting fibrosis (Bujak and Frangogiannis 2007). Although the inflammatory reaction is critically involved in post-infarction reparative fibrosis (Frangogiannis 2006a), (Frangogiannis 2008) the mechanistic basis of fibrotic cardiac remodeling in response to injurious stimuli that do not result in cardiomyocyte death remains poorly understood.

Pressure overload induced by hypertension or aortic stenosis results in extensive fibrotic remodeling of the heart (Heymans et al. 2005), (Cingolani et al. 2004), initially associated with diastolic dysfunction that frequently progresses to ventricular dilation and combined diastolic and systolic heart failure (Berk et al. 2007). The availability of a murine model of transverse aortic constriction (TAC) provides us with a valuable tool to explore the mechanisms involved in cardiac fibrosis following pressure overload using genetically targeted animals. However, exploration of the pathogenesis of fibrotic cardiac remodeling requires detailed characterization of the inflammatory and fibrotic response in pressure-overloaded mouse hearts. Our investigation examines the time course of cellular and molecular events leading to transition from inflammation to myocardial fibrosis in mice undergoing TAC protocols. Despite the absence of significant cardiomyocyte loss, pressure overload triggers a transient inflammatory reaction, associated with chemokine and cytokine upregulation and recruitment of macrophages, but not neutrophils, in the murine heart. Induction of pro-inflammatory cytokines activates inhibitory mediators, such as TGF-β, that suppress inflammation, but also promote interstitial and perivascular fibrosis. Because pressure overload is not associated with significant cardiomyocyte loss, TGF-β-mediated matrix deposition has no reparative function and is maladaptive. Fibrotic remodeling of the ventricle is initially associated with marked hypertrophy without ventricular enlargement or systolic functional impairment, followed by the development of chamber dilation and systolic dysfunction. Characterization of the inflammatory and fibrotic response in the murine pressure-overloaded heart will facilitate mechanistic studies using genetically targeted animals to explore the pathogenesis of cardiac fibrosis.

Materials and Methods

1. Animal protocols

Animal experiments were approved by the Baylor College of Medicine Institutional Review Board. All animals received humane care in compliance with the “Principle of laboratory and animal care” (NIH publication No 86-23, revised 1985). Male and female, 3-5 month-old C57/BL/6 mice (Jackson laboratories) were anesthetized by an intraperitoneal injection of sodium pentobarbital (60 μg/g). Aortic banding was achieved by creating a constriction between the right innominate and left carotid arteries. A 6-0 suture was tied twice around a blunt 3-mm segment of a 27-gauge needle, which was positioned adjacent to the aorta and was removed after placement of the ligature. The degree of pressure overload was measured by right-to-left carotid artery flow velocity ratio after constricting the transverse aorta. Only mice with a flow ratio from 5:1 to 10:1 were used for analysis. At the end of the experiment, the heart was excised, fixed in zinc-formalin, and embedded in paraffin for histological studies, or frozen for RNA/protein isolation. Animals used for histology underwent 3, 7, and 28 days of banding (n=8/group). Mice used for RNA extraction underwent 3 (n=7) or 7 days (n=4) of banding. An additional group of mice (n=7) was used for protein extraction after 7 days of TAC. As a control, a “sham” operation without aortic constriction was performed on age-matched mice (histology n=6, RNA n=6, protein n=8).

2. Immunohistochemistry and quantitative histology

Zinc-formalin-fixed sections were cut at 5 μm and stained immunohistochemically with the following antibodies: mouse anti-α–smooth muscle actin (α-SMA) (Sigma, St. Louis, MO) rat anti-mouse macrophage Mac-2 (Cedarlane, Burlington NC), rat anti-neutrophil (Serotec, Raleigh NC), rat anti-mouse CD31 (Pharmingen, San Diego, CA), and rabbit anti-mouse tenascin-C antibody (R&D Systems). Staining was performed using a peroxidase-based technique with the Vectastain ELITE kit (Vector, Burlingame, CA) and developed with diaminobenzidine+nickel (Vector) (Zymek et al. 2006), (Gersch et al. 2002). Subsequently the sections were counterstained with eosin. The MOM kit (Vector) was used for α-SMA staining. For CD31 staining, the Tyramide Signal Amplification kit (Perkin Elmer, Boston, MA) was used on trypsin-pretreated sections (Zymek et al. 2006). All staining techniques were validated using appropriate negative and positive controls. Negative controls included sections stained after omission of the primary antibody. Sections from mouse infarcts that contain large numbers of neutrophils, macrophages, myofibroblasts and vascular cells (Dewald et al. 2004), and express large amounts of tenascin-C (Bujak et al. 2007) were used as positive controls. Assessment of neutrophil and macrophage density was performed by counting the number of neutrophils and Mac-2-immunoreactive cells respectively (Dewald et al. 2005). Quantitation of the tenascin-C-stained area was performed in four fields from two sections from each animal. Tenascin-C staining was expressed as a percentage of the total myocardial area. The collagen network was identified using picrosirius red staining (Dewald et al. 2005). Assessment of the percentage of the collagen-stained area was performed in basal, mid-ventricular and apical segments of the left ventricle and in the right ventricle using ImagePro software. Nine high-power fields were used for each segment. Microvascular density was assessed by counting the number of CD31-positive profiles in the endocardial and epicardial segment of the left ventricular free wall, the septum and the right ventricle. Four high-power fields were used for analysis of each segment. In order to quantitate the development of perivascular fibrosis in pressure-overloaded hearts, arterioles that were cut in cross-section were scanned. The media and the adventitia were traced and the ratio of the adventitial to the medial area (A/M) was measured. Ten random arterioles were used for analysis in each animal.

3. Ribonuclease protection assay (RPA)

Inflammatory gene expression in murine hearts was assessed using an RPA (RiboQuant; Pharmingen) (Dewald et al. 2005), (Gersch et al. 2002). mRNA expression levels of the chemokines Macrophage Inflammatory Protein (MIP)-1α, MIP-1β, MIP-2, Monocyte Chemoattractant Protein (MCP)-1, Interferon-γ-inducible Protein (IP)-10, lymphotactin, T cell activation protein (TCA)-3 and eotaxin, the cytokines Tumor Necrosis Factor (TNF)-α, Interleukin (IL)-1β, IL-6, and IL-10, and TGF-β1, -β2, and -β3, and the matricellular protein Osteopontin were determined as previously described (Dewald et al. 2005). The signals were quantified using Image QuaNT software and normalized to the ribosomal protein L32 mRNA. Unprotected probes were loaded as size markers.

4. Protein extraction and western blotting

Protein was isolated from whole hearts (sham, 7 days TAC). Western blotting with rabbit anti-Smad2, anti-p-Smad2, anti-p-Smad1/5, and anti-Smad1/5 (Cell Signaling, Beverly, MA) was performed as previously described (Bujak et al. 2007). Protein extracted from TGF-β-stimulated mouse cardiac fibroblasts was used as a positive control (Bujak et al. 2007), (Bujak et al. 2008b).

5. Echocardiographic analysis

Short axis M-mode echocardiography was performed prior to the surgical procedure and before the end of each experiment (3, 7 or 28 days of TAC) using a 13 MHz probe (Sequoia C256;

Acuson, Mountain View, CA) (Bujak et al. 2008a). The following parameters were measured as indicators of function and remodeling: left ventricular end-diastolic diameter (LVEDD), left ventricular end-systolic diameter (LVESD), fractional shortening (FS=[LVEDD-LVESD] ×100/LVEDD), interventricular septal (IVS) thickness, posterior wall (PW) thickness and left ventricular mass (LV mass= $1.05(\text{IVS thickness} + \text{LVEDD} + \text{PW thickness})^3 - \text{LVEDD}^3$ (Collins et al. 2003).

6. Statistical analysis

Statistical analysis was performed using ANOVA followed by t-test corrected for multiple comparisons (Student-Newman-Keuls). Paired t-test was used to compare echocardiographic endpoints before instrumentation and after TAC. Data were expressed as mean ± SEM. Statistical significance was set at 0.05.

Results

1. Cytokine induction in the pressure-overloaded heart

Pressure overload triggers a transient inflammatory response in the myocardium associated with increased expression of pro-inflammatory cytokines. Sham-operated hearts exhibited negligible mRNA expression of TNF-α, IL-1β and IL-6. After 3 days of TAC significant TNF-α and IL-1β mRNA upregulation was noted in the pressure-overloaded heart; in contrast, IL-6 expression remained low (Fig. 1). After 7 days of aortic banding, TNF-α and IL-1β expression returned to sham levels.

2. Chemokine induction in the pressure-overloaded heart

Several members of the chemokine family were upregulated in the pressure overloaded heart. Sham-operated hearts exhibited low level expression of MCP-1 (MCP-1:L32 ratio:0.043 ±0.0021) and MIP-2 mRNA (MIP-2:L32 ratio 0.023±0.02), but negligible expression of IP-10, MIP-1α, MIP-1β, TCA-3 and eotaxin message (<1% of L32 levels). After 7 days of TAC significant induction of MIP-2, IP-10 and MCP-1 was noted (Fig. 2). In contrast, cardiac mRNA levels of MIP-1α, MIP-1β, lymphotactin, TCA-3 and eotaxin remained low (ratio to L32<0.01).

3. Leukocyte infiltration in the pressure-overloaded heart

Upregulation of pro-inflammatory mediators was associated with infiltration of the pressure-overloaded myocardium with leukocytes. A modest increase in myocardial neutrophil density was noted after 3 days of TAC, but did not reach statistical significance (Fig. 3). On the other hand, macrophage density was markedly increased in the pressure-overloaded heart after 7 days of TAC (Fig. 3B, E). Partial resolution of the macrophage infiltrate was observed after 28 days of aortic banding (Fig. 3C-E).

4. Fibrotic remodeling of the pressure-overloaded ventricle

In the pressure-overloaded heart the inflammatory response was associated with induction of matricellular proteins followed by the development of diffuse fibrosis. Perivascular and interstitial infiltration with spindle-shaped α-SMA-positive myofibroblasts was noted after 7 days of TAC (Fig. 4A). The matricellular proteins osteopontin and tenascin-C were markedly induced in the pressure-overloaded ventricle. Induction of osteopontin mRNA was noted after 3 days of TAC (Fig. 4B). Extensive deposition of tenascin-C (Fig. 4C-D), a marker of active interstitial remodeling (Frangogiannis et al. 2002), was observed after 7 days, but significantly decreased after 28 days (Fig. 4C) of aortic banding. Sirius red-stained area significantly increased in the pressure-overloaded heart after 3-28 days of aortic banding, peaking at 7 days (Fig. 4F, G). Marked expansion of the cardiac interstitium was noted in both the left and right

ventricular myocardium and was comparable in basal, mid-ventricular and apical segments (Fig. 4G).

5. Perivascular inflammatory and fibrotic changes in the pressure-overloaded heart

Inflammatory and fibrotic changes in the pressure-overloaded heart were predominantly localized in perivascular areas. After 7 days of TAC, cardiac arterioles showed marked perivascular inflammation and expansion of the adventitia (Fig. 5B-E), associated with macrophage (Fig. 5C) and myofibroblast infiltration. The ratio of the arteriolar adventitial to medial area (A:M) markedly increased after 7-28 days of aortic banding (Fig. 5F). After 28 days of TAC, deposition of dense collagen fibers was noted in the arteriolar adventitia (Fig. 5E).

6. Induction of TGF-β isoforms and activation of TGF-β signaling in the pressure-overloaded heart

Because TGF-β plays a crucial role in the transition from inflammation to fibrosis we examined the time course of TGF-β isoform expression in the pressure-overloaded heart. Fibrotic remodeling of the ventricle was associated with marked upregulation of TGF-β1, -β2 and -β3 mRNA after 7 days of TAC (Fig. 6A-C) and with activation of TGF-β signaling evidenced by markedly increased levels of p-Smad2 and p-Smad1 (Fig. 6D-E).

7. Effects of pressure overload on cardiac microvascular density

In sham-operated hearts, the density of CD31-positive vessels (Fig. 7) was significantly lower in the right ventricular myocardium when compared to the left ventricle (Fig. 7D). The number of microvascular profiles was comparable in subendocardial and subepicardial areas of the left ventricle (Fig. 7D). After 3 days of TAC, microvascular density significantly increased in all left ventricular myocardial segments. Microvascular density in both right and left ventricular myocardium peaked after 7 days and remained elevated after 28 days of aortic banding (Fig. 7D).

8. TAC induces cardiac hypertrophy followed by ventricular dilation and systolic dysfunction

The inflammatory and fibrotic changes in the pressure-overloaded heart were associated with alterations in chamber dimensions and progressive impairment of left ventricular function. After 3-7 days of TAC, the hearts exhibited marked concentric hypertrophy (Fig. 8), but had preserved systolic function (Table 1). LV mass was markedly increased; however, chamber dimensions (LVEDD and LVESD) remained normal, and fractional shortening was preserved (Table 1). After 28 days of aortic banding, LV mass increased further, and the hypertrophied heart developed systolic dysfunction (suggested by a significant reduction in FS) and dilative remodeling (indicated by a marked increase in LVESD) (Fig. 8C, Table 1).

Discussion

The availability of genetically targeted mice has revolutionized biomedical research providing unique opportunities to study the role of specific mediators in complex pathobiological processes. However, dissection of the mechanistic basis of a pathophysiologic condition requires knowledge of the time course of cellular and molecular events in carefully designed mouse models of disease. Our study describes in detail the cardiac inflammatory and fibrotic response in a mouse model of cardiac pressure overload due to TAC. The findings provide the necessary foundations for mechanistic studies using genetically targeted animals to explore the role of inflammatory mediators in the development of fibrous tissue deposition and cardiac dysfunction in the pressure-overloaded heart.

Cardiomyocyte necrosis activates innate immune mechanisms triggering a potent inflammatory reaction that ultimately results in reparative fibrosis. Evolving evidence suggests that cardiac insults that do not cause cardiomyocyte death, such as pressure overload, are also capable of inducing an inflammatory reaction in the myocardium. Several distinct mechanisms may be involved in activation of the inflammatory response in the pressure overloaded heart. Neurohormonal activation may directly stimulate inflammatory pathways through generation of reactive oxygen species and activation of the NF-κB system. Angiotensin II and aldosterone enhance NF-κB activity exerting direct pro-inflammatory effects on the myocardium (Muller et al. 2000), (Sun et al. 2002). On the other hand pressure overload may induce alterations in cardiac extracellular matrix through activation of Matrix Metalloproteinases (MMPs). Matrix fragments may serve as “danger signals” that activate Toll-Like Receptors (TLRs), triggering inflammatory mediator synthesis in the pressure-overloaded myocardium (Beg 2002).

Although the inflammatory reactions following infarction and pressure overload share many common characteristics, they also have significant differences. Compared with the rapid upregulation of a broad spectrum of inflammatory mediators in myocardial infarction (Dewald et al. 2004), pressure overload induces only a subgroup of inflammatory chemokines and cytokines. IL-6, MIP-1α and MIP-1β expression is markedly upregulated in healing infarcts (Dewald et al. 2004), but not in pressure-overloaded hearts. In addition, abundant infiltration of the myocardium with neutrophils is noted in infarction, but not following aortic constriction. The intense inflammatory reaction in the infarcted myocardium probably reflects the rapid activation of several distinct proinflammatory pathways (such as the complement cascade, reactive oxygen and TLR-mediated pathways) following cardiomyocyte necrosis. In contrast, in the pressure-overloaded ventricle, the late induction of chemokine synthesis (Fig. 2) appears to be more consistent with delayed pro-inflammatory effects of neurohormonal mediators.

What is the role of inflammatory mediators in fibrotic remodeling of the pressure-overloaded ventricle? Pro-inflammatory cytokines are highly pleiotropic and may regulate the fibrotic process through several distinct pathways. Both TNF-α and IL-1β decrease collagen synthesis and enhance MMP expression and activity in cardiac fibroblasts (Siwik and Colucci 2004), (Li et al. 2002), (Brown et al. 2007) inducing matrix degradation (Siwik et al. 2000). However, TNF-α and IL-1β also stimulate expression of growth factors (such as TGF-β) that promote matrix deposition. The relative significance of these properties in the pathogenesis of cardiac fibrosis remains poorly understood. Transgenic mice with cardiac-specific overexpression of TNF-α develop heart failure (Bryant et al. 1998) associated with increased collagen deposition and denaturation, and enhanced MMP activity (Li et al. 2000). Enhanced fibrosis in TNF-α–overexpressing animals is associated with increased expression of TGF-β isoforms (Sivasubramanian et al. 2001). These findings suggest that TNF-α mediates fibrotic changes, while enhancing matrix-degrading activity. TNF-α null mice on the other hand exhibited reduced fibrosis and decreased MMP-9 activity following aortic constriction suggesting that this cytokine is an important profibrotic mediator in the pressure-overloaded heart (Sun et al. 2007). In contrast, the role of IL-1 signaling in fibrotic remodeling of the pressure-overloaded heart has not been investigated.

Chemokines, such as MCP-1 may also play an important role in the pathogenesis of cardiac fibrosis (Frangogiannis et al. 2007). MCP-1 mRNA expression was induced in a rat model of pressure overload due to suprarenal aortic constriction. Chronic MCP-1 neutralization attenuated fibrosis, but not cardiomyocyte hypertrophy, and ameliorated diastolic dysfunction without affecting systolic function (Kuwahara et al. 2004). In the cardiomyopathic heart MCP-1 may mediate its pro-fibrotic effects through recruitment of mononuclear cells that may serve as an important source of fibrogenic mediators. In addition, MCP-1 may directly modulate fibroblast phenotype and activity (Kruglov et al. 2006), (Gharaee-Kermani et al. 1996) and may be involved in recruitment of fibrocytes, a circulating population of cells that

share leukocyte and mesenchymal markers, and are capable of myofibroblast differentiation (Quan et al. 2004), (Wynn 2008).

However, activation of inflammatory pathways in the pressure-overloaded heart is a transient event, followed by resolution of the leukocyte infiltrate and development of fibrosis. Induction of pro-inflammatory mediators triggers “stop signals” capable of suppressing acute inflammation. In the reparative response following myocardial infarction, TGF-β appears to play an important role as an inhibitory mediator, suppressing pro-inflammatory cytokine synthesis (Bujak and Frangogiannis 2007), (Ikeuchi et al. 2004), while promoting extracellular matrix deposition (Bujak and Frangogiannis 2007), (Lutgens et al. 2002). Although in the infarcted myocardium the anti-inflammatory and profibrotic actions of TGF-β may bridge the inflammatory and the reparative phase of healing, in the pressure-overloaded heart, TGF-β-mediated matrix deposition, in the absence of significant cardiomyocyte loss, is clearly maladaptive. Activation of TGF-β signaling pathways in the pressure-overloaded heart may suppress inflammation, but at a heavy cost, resulting in fibrotic remodeling of the ventricle. Thus, dissection of the signaling pathways responsible for the anti-inflammatory and pro-fibrotic actions of TGF-β is crucial for designing optimal therapeutic strategies that attenuate fibrosis without interfering with resolution of inflammation. We demonstrated activation of both the Smad2/3 and the Smad1/5 pathways in the pressure overloaded myocardium (Fig. 6). Smad3 signaling appears to play an essential role in remodeling of the infarcted heart, in part by mediating TGF-β-induced expression of matrix proteins by border zone fibroblasts (Bujak et al. 2007). On the other hand, activation of the Smad1 pathway has been suggested as a Smad3-independent mode of TGF-β signaling that may operate in chronic fibrotic disorders (Pannu et al. 2007). The role of these pathways in mediating anti-inflammatory and profibrotic actions in the pressure-overloaded heart remains unknown.

Cardiac fibrosis following pressure overload is associated with extensive vascular remodeling. Microvascular density significantly increases after 3-28 days of TAC (Fig. 7); increased perfusion may be needed to meet the demands of the hypertrophied myocardium and to ensure delivery of nutrients to the cells involved in fibrotic remodeling. Thus, angiogenesis accompanies the development of fibrosis and may be essential for fibroblast growth (Strieter et al. 2007). In addition, myocardial arterioles actively participate in the fibrotic process. Pressure overload results in adventitial inflammation followed by extensive periarteriolar fibrosis (Fig. 5), reflecting the prominent role of the proinflammatory and profibrotic effects of local angiotensin II on vascular and adventitial cells (McEwan et al. 1998), (Lee et al. 1995).

Our quantitative analysis seems to indicate that collagen deposition peaks after 7 days and may somewhat decrease after 28 days of TAC (Fig. 4G). However, these findings should not be interpreted as indicative of reversal of fibrosis. In order to study the extent of collagen deposition in sections from the pressure-overloaded heart we quantitatively assessed the area stained for Sirius red. Because Sirius red also binds to non-collagenous proteins containing basic amino acids, the technique is not specific for collagen unless polarized light microscopy is performed (Junqueira et al. 1979), (Nielsen et al. 1998). In addition, quantitation of the collagen content in the heart using a hydroxyproline assay was not performed. Although our findings accurately illustrate the expansion of the cardiac interstitial space following TAC, quantitative analysis of the Sirius red-stained area does not directly reflect the amount of collagen in the pressure-overloaded heart.

The time course of cellular events in fibrotic remodeling of the pressure-overloaded heart suggests a transition from an inflammatory to a fibrotic response. Early inflammatory mediator upregulation may be triggered by neurohormonal pathways and ultimately results in activation of signals that suppress inflammation, while promoting matrix deposition. The detailed

characterization of cardiac fibrosis due to aortic constriction in the mouse provides us with a great tool to investigate the mechanisms involved in fibrotic remodeling of the pressure-overloaded heart.

Acknowledgments

Supported by NIH R01 HL-76246 and HL-85440.

References

Beg AA. Endogenous ligands of Toll-like receptors: implications for regulating inflammatory and immune responses. Trends Immunol 2002;23:509–512. [PubMed: 12401394]

Berk BC, Fujiwara K, Lehoux S. ECM remodeling in hypertensive heart disease. J Clin Invest 2007;117:568–575. [PubMed: 17332884]

Brown RD, Ambler SK, Mitchell MD, Long CS. The cardiac fibroblast: therapeutic target in myocardial remodeling and failure. Annu Rev Pharmacol Toxicol 2005;45:657–687. [PubMed: 15822192]

Brown RD, Jones GM, Laird RE, Hudson P, Long CS. Cytokines regulate matrix metalloproteinases and migration in cardiac fibroblasts. Biochem Biophys Res Commun 2007;362:200–205. [PubMed: 17706606]

Bryant D, Becker L, Richardson J, Shelton J, Franco F, Peshock R, Thompson M, Giroir B. Cardiac failure in transgenic mice with myocardial expression of tumor necrosis factor-alpha. Circulation 1998;97:1375–1381. [PubMed: 9577949]

Bujak M, Dobaczewski M, Chatila K, Mendoza LH, Li N, Reddy A, Frangogiannis NG. Interleukin-1 receptor type I signaling critically regulates infarct healing and cardiac remodeling. Am J Pathol 2008a; 173:57–67. [PubMed: 18535174]

Bujak M, Frangogiannis NG. The role of TGF-beta signaling in myocardial infarction and cardiac remodeling. Cardiovasc Res 2007;74:184–195. [PubMed: 17109837]

Bujak M, Kweon HJ, Chatila K, Li N, Taffet G, Frangogiannis NG. Aging-related defects are associated with adverse cardiac remodeling in a mouse model of reperfused myocardial infarction. J Am Coll Cardiol 2008b;51:1384–1392. [PubMed: 18387441]

Bujak M, Ren G, Kweon HJ, Dobaczewski M, Reddy A, Taffet G, Wang XF, Frangogiannis NG. Essential Role of Smad3 in Infarct Healing and in the Pathogenesis of Cardiac Remodeling. Circulation 2007;116:2127–2138. [PubMed: 17967775]

Cingolani OH, Yang XP, Liu YH, Villanueva M, Rhaleb NE, Carretero OA. Reduction of cardiac fibrosis decreases systolic performance without affecting diastolic function in hypertensive rats. Hypertension 2004;43:1067–1073. [PubMed: 15023934]

Cleutjens JP, Verluyten MJ, Smiths JF, Daemen MJ. Collagen remodeling after myocardial infarction in the rat heart. Am J Pathol 1995;147:325–338. [PubMed: 7639329]

Collins KA, Korcarz CE, Lang RM. Use of echocardiography for the phenotypic assessment of genetically altered mice. Physiol Genomics 2003;13:227–239. [PubMed: 12746467]

Dewald O, Ren G, Duerr GD, Zoerlein M, Klemm C, Gersch C, Tincey S, Michael LH, Entman ML, Frangogiannis NG. Of mice and dogs: species-specific differences in the inflammatory response following myocardial infarction. Am J Pathol 2004;164:665–677. [PubMed: 14742270]

Dewald O, Zymek P, Winkelmann K, Koerting A, Ren G, Abou-Khamis T, Michael LH, Rollins BJ, Entman ML, Frangogiannis NG. CCL2/Monocyte Chemoattractant Protein-1 regulates inflammatory responses critical to healing myocardial infarcts. Circ Res 2005;96:881–889. [PubMed: 15774854]

Frangogiannis NG. The immune system and cardiac repair. Pharmacol Res 2008;58:88–111. [PubMed: 18620057]

Frangogiannis NG. The mechanistic basis of infarct healing. Antioxid Redox Signal 2006a;8:1907–1939. [PubMed: 17034340]

Frangogiannis NG. Targeting the inflammatory response in healing myocardial infarcts. Curr Med Chem 2006b;13:1877–1893. [PubMed: 16842199]

Frangogiannis NG, Dewald O, Xia Y, Ren G, Haudek S, Leucker T, Kraemer D, Taffet G, Rollins BJ, Entman ML. Critical role of monocyte chemoattractant protein-1/CC chemokine ligand 2 in the pathogenesis of ischemic cardiomyopathy. Circulation 2007;115:584–592. [PubMed: 17283277]

Frangogiannis NG, Shimoni S, Chang SM, Ren G, Dewald O, Gersch C, Shan K, Aggeli C, Reardon M, Letsou GV, Espada R, Ramchandani M, Entman ML, Zoghbi WA. Active interstitial remodeling: an important process in the hibernating human myocardium. J Am Coll Cardiol 2002;39:1468–1474. [PubMed: 11985909]

Gersch C, Dewald O, Zoerlein M, Michael LH, Entman ML, Frangogiannis NG. Mast cells and macrophages in normal C57/BL/6 mice. Histochem Cell Biol 2002;118:41–49. [PubMed: 12122446]

Gharaee-Kermani M, Denholm EM, Phan SH. Costimulation of fibroblast collagen and transforming growth factor beta1 gene expression by monocyte chemoattractant protein-1 via specific receptors. J Biol Chem 1996;271:17779–17784. [PubMed: 8663511]

Heymans S, Schroen B, Vermeersch P, Milting H, Gao F, Kassner A, Gillijns H, Herijgers P, Flameng W, Carmeliet P, Van de Werf F, Pinto YM, Janssens S. Increased cardiac expression of tissue inhibitor of metalloproteinase-1 and tissue inhibitor of metalloproteinase-2 is related to cardiac fibrosis and dysfunction in the chronic pressure-overloaded human heart. Circulation 2005;112:1136–1144. [PubMed: 16103240]

Ikeuchi M, Tsutsui H, Shiomi T, Matsusaka H, Matsushima S, Wen J, Kubota T, Takeshita A. Inhibition of TGF-beta signaling exacerbates early cardiac dysfunction but prevents late remodeling after infarction. Cardiovasc Res 2004;64:526–535. [PubMed: 15537506]

Janicki JS, Brower GL. The role of myocardial fibrillar collagen in ventricular remodeling and function. J Card Fail 2002;8:S319–325. [PubMed: 12555139]

Junqueira LC, Bignolas G, Brentani RR. Picrosirius staining plus polarization microscopy, a specific method for collagen detection in tissue sections. Histochem J 1979;11:447–455. [PubMed: 91593]

Khan R, Sheppard R. Fibrosis in heart disease: understanding the role of transforming growth factor-beta in cardiomyopathy, valvular disease and arrhythmia. Immunology 2006;118:10–24. [PubMed: 16630019]

Kruglov EA, Nathanson RA, Nguyen T, Dranoff JA. Secretion of MCP-1/CCL2 by bile duct epithelia induces myofibroblastic transdifferentiation of portal fibroblasts. Am J Physiol Gastrointest Liver Physiol 2006;290:G765–771. [PubMed: 16282363]

Kuwahara F, Kai H, Tokuda K, Takeya M, Takeshita A, Egashira K, Imaizumi T. Hypertensive myocardial fibrosis and diastolic dysfunction: another model of inflammation? Hypertension 2004;43:739–745. [PubMed: 14967845]

Lee AA, Dillmann WH, McCulloch AD, Villarreal FJ. Angiotensin II stimulates the autocrine production of transforming growth factor-beta 1 in adult rat cardiac fibroblasts. J Mol Cell Cardiol 1995;27:2347–2357. [PubMed: 8576949]

Li J, Schwimmbeck PL, Tschope C, Leschka S, Husmann L, Rutschow S, Reichenbach F, Noutsias M, Kobalz U, Poller W, Spillmann F, Zeichhardt H, Schultheiss HP, Pauschinger M. Collagen degradation in a murine myocarditis model: relevance of matrix metalloproteinase in association with inflammatory induction. Cardiovasc Res 2002;56:235–247. [PubMed: 12393094]

Li YY, Feng YQ, Kadokami T, McTiernan CF, Draviam R, Watkins SC, Feldman AM. Myocardial extracellular matrix remodeling in transgenic mice overexpressing tumor necrosis factor alpha can be modulated by anti-tumor necrosis factor alpha therapy. Proc Natl Acad Sci U S A 2000;97:12746–12751. [PubMed: 11070088]

Lutgens E, Gijbels M, Smook M, Heeringa P, Gotwals P, Koteliansky VE, Daemen MJ. Transforming growth factor-beta mediates balance between inflammation and fibrosis during plaque progression. Arterioscler Thromb Vasc Biol 2002;22:975–982. [PubMed: 12067907]

McEwan PE, Gray GA, Sherry L, Webb DJ, Kenyon CJ. Differential effects of angiotensin II on cardiac cell proliferation and intramyocardial perivascular fibrosis in vivo. Circulation 1998;98:2765–2773. [PubMed: 9851965]

Muller DN, Dechend R, Mervaala EM, Park JK, Schmidt F, Fiebeler A, Theuer J, Breu V, Ganten D, Haller H, Luft FC. NF-kappaB inhibition ameliorates angiotensin II-induced inflammatory damage in rats. Hypertension 2000;35:193–201. [PubMed: 10642297]

Nielsen LF, Moe D, Kirkeby S, Garbarsch C. Sirius red and acid fuchsin staining mechanisms. Biotech Histochem 1998;73:71–77. [PubMed: 9605621]

Pannu J, Nakerakanti S, Smith E, ten Dijke P, Trojanowska M. Transforming growth factor-beta receptor type I-dependent fibrogenic gene program is mediated via activation of Smad1 and ERK1/2 pathways. J Biol Chem 2007;282:10405–10413. [PubMed: 17317656]

Quan TE, Cowper S, Wu SP, Bockenstedt LK, Bucala R. Circulating fibrocytes: collagen-secreting cells of the peripheral blood. Int J Biochem Cell Biol 2004;36:598–606. [PubMed: 15010326]

Sivasubramanian N, Coker ML, Kurrelmeyer KM, MacLellan WR, DeMayo FJ, Spinale FG, Mann DL. Left ventricular remodeling in transgenic mice with cardiac restricted overexpression of tumor necrosis factor. Circulation 2001;104:826–831. [PubMed: 11502710]

Siwik DA, Chang DL, Colucci WS. Interleukin-1beta and tumor necrosis factor-alpha decrease collagen synthesis and increase matrix metalloproteinase activity in cardiac fibroblasts in vitro. Circ Res 2000;86:1259–1265. [PubMed: 10864917]

Siwik DA, Colucci WS. Regulation of matrix metalloproteinases by cytokines and reactive oxygen/nitrogen species in the myocardium. Heart Fail Rev 2004;9:43–51. [PubMed: 14739767]

Strieter RM, Gomperts BN, Keane MP. The role of CXC chemokines in pulmonary fibrosis. J Clin Invest 2007;117:549–556. [PubMed: 17332882]

Sun M, Chen M, Dawood F, Zurawska U, Li JY, Parker T, Kassiri Z, Kirshenbaum LA, Arnold M, Khokha R, Liu PP. Tumor necrosis factor-alpha mediates cardiac remodeling and ventricular dysfunction after pressure overload state. Circulation 2007;115:1398–1407. [PubMed: 17353445]

Sun Y, Zhang J, Lu L, Chen SS, Quinn MT, Weber KT. Aldosterone-induced inflammation in the rat heart: role of oxidative stress. Am J Pathol 2002;161:1773–1781. [PubMed: 12414524]

Wynn TA. Cellular and molecular mechanisms of fibrosis. J Pathol 2008;214:199–210. [PubMed: 18161745]

Zymek P, Bujak M, Chatila K, Cieslak A, Thakker G, Entman ML, Frangogiannis NG. The role of platelet-derived growth factor signaling in healing myocardial infarcts. J Am Coll Cardiol 2006;48:2315–2323. [PubMed: 17161265]

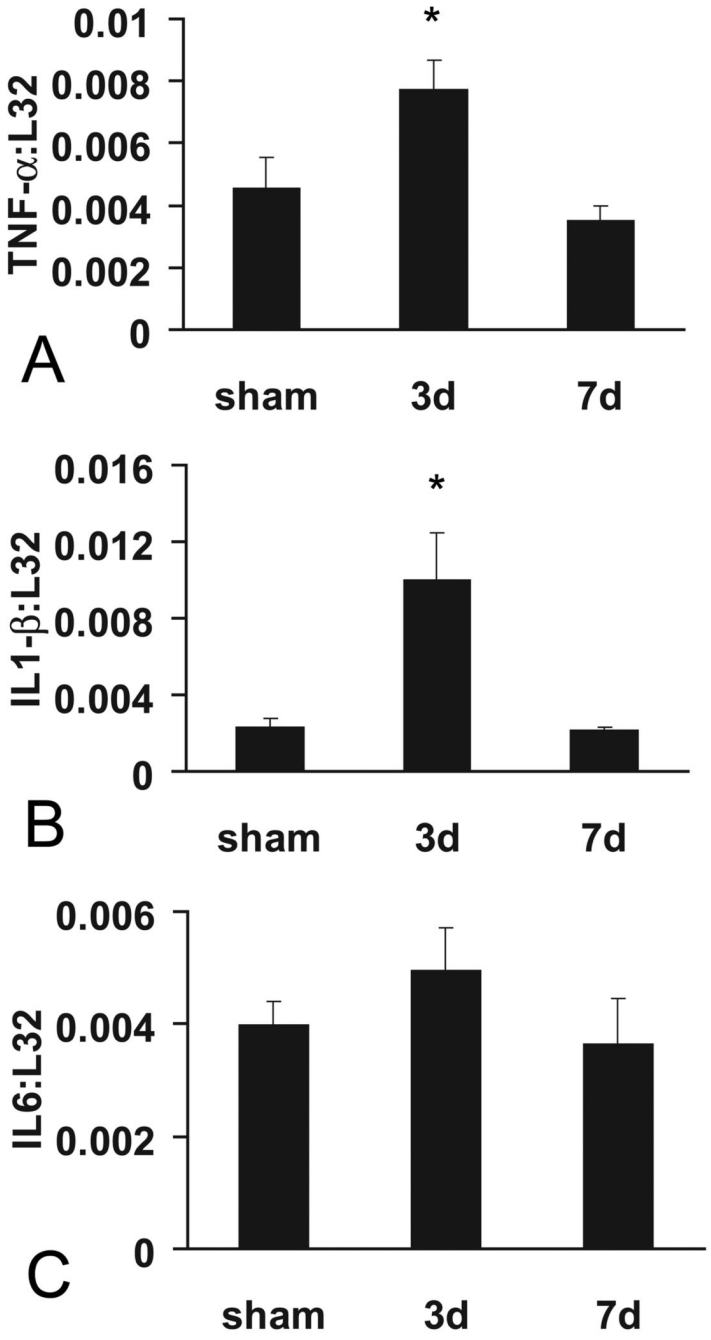

Figure 1.

Induction of proinflammatory cytokines in the pressure-overloaded myocardium. RPA analysis demonstrated upregulation of TNF-α (A), and IL-1β (B) mRNA after 3days of aortic banding (*p<0.05 vs. sham). TNF-α and IL-1β mRNA expression returned to sham levels after 7 days of TAC. IL-6 mRNA expression was not induced in the pressure-overloaded heart (C).

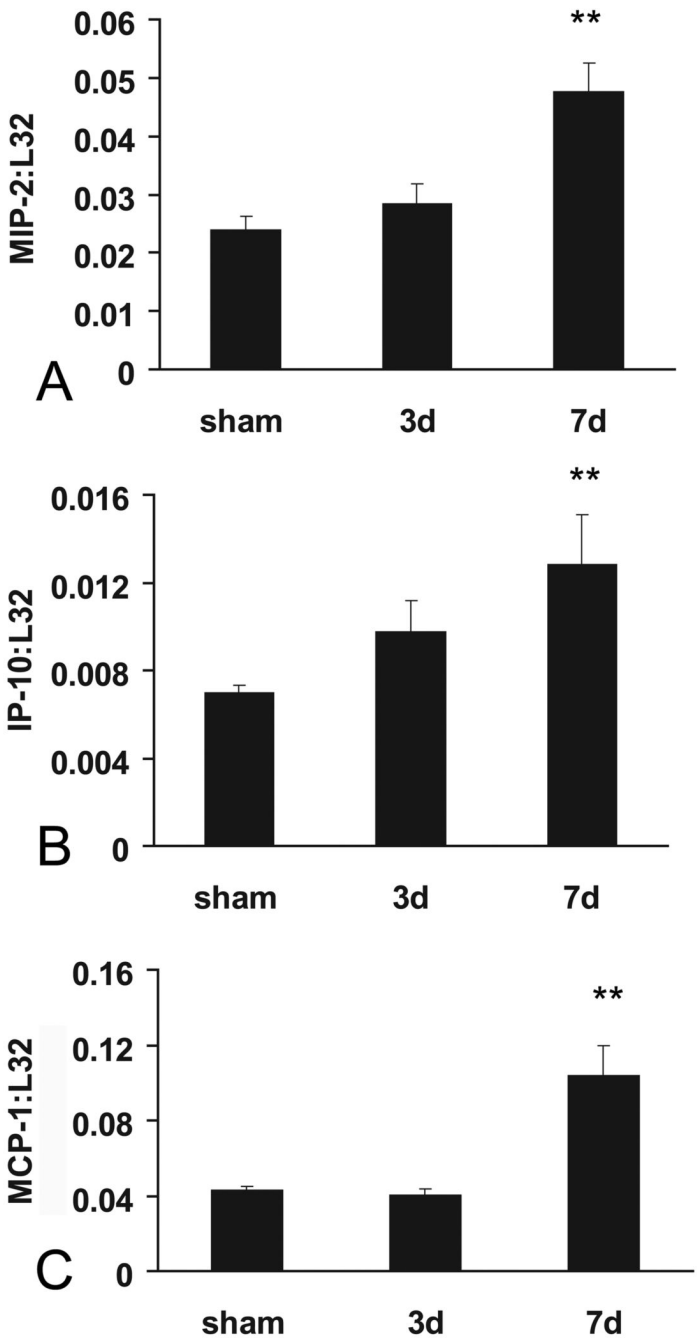

Figure 2.

Chemokine upregulation in the pressure-overloaded mouse heart. RPA analysis demonstrated that mRNA expression of the CXC chemokines MIP-2 (A) and IP-10 (B) and the CC chemokine MCP-1 (C) was induced after 7 days of TAC (**p<0.01 vs. sham).

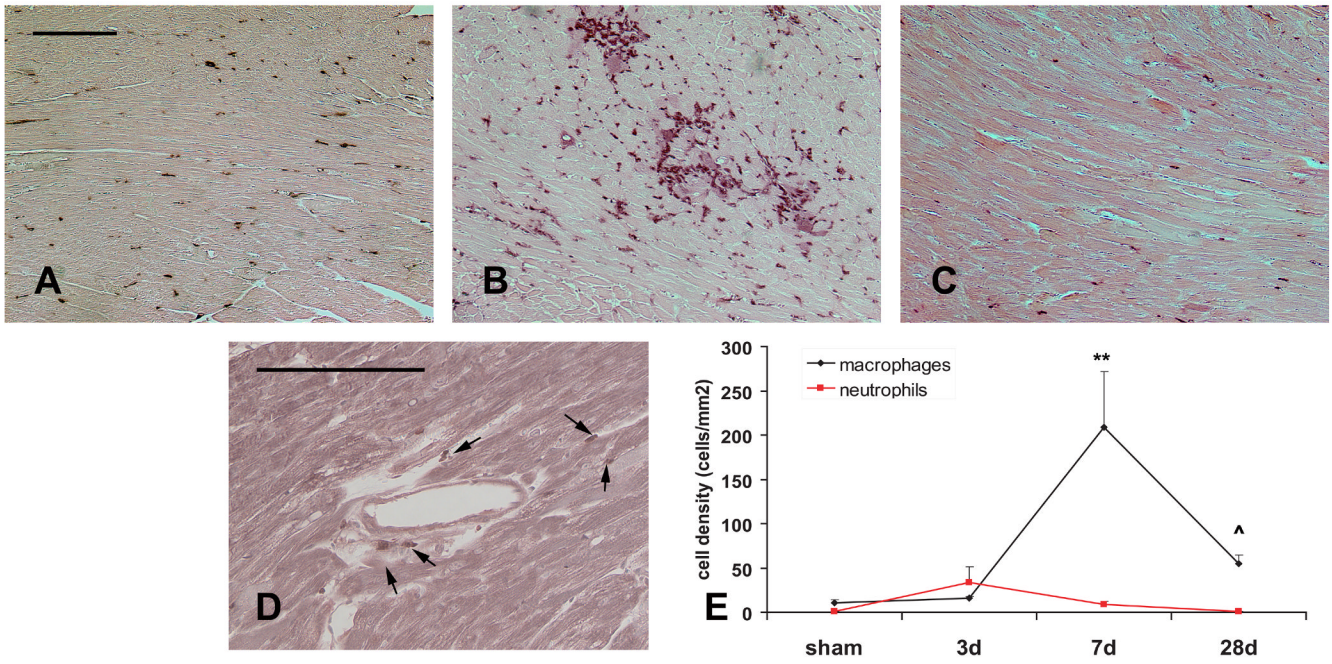

Figure 3.

The time course of leukocyte infiltration in the pressure-overloaded mouse heart. Mac-2 immunohistochemistry identified macrophages in the heart after 3 days (A), 7 days (B) and 28 days (C) of TAC. Macrophage density peaked after 7 days of aortic banding (E, **$p<0.01$ vs. sham). Partial resolution of the macrophage infiltrate was noted after 28 days of aortic constriction (^$p<0.05$ vs. 7days). In contrast, only modest infiltration of the pressure overloaded myocardium with neutrophils (arrows) was noted after 3 days of TAC (D). The increase in neutrophil density did not reach statistical significance (E). Scale bar=100μm.

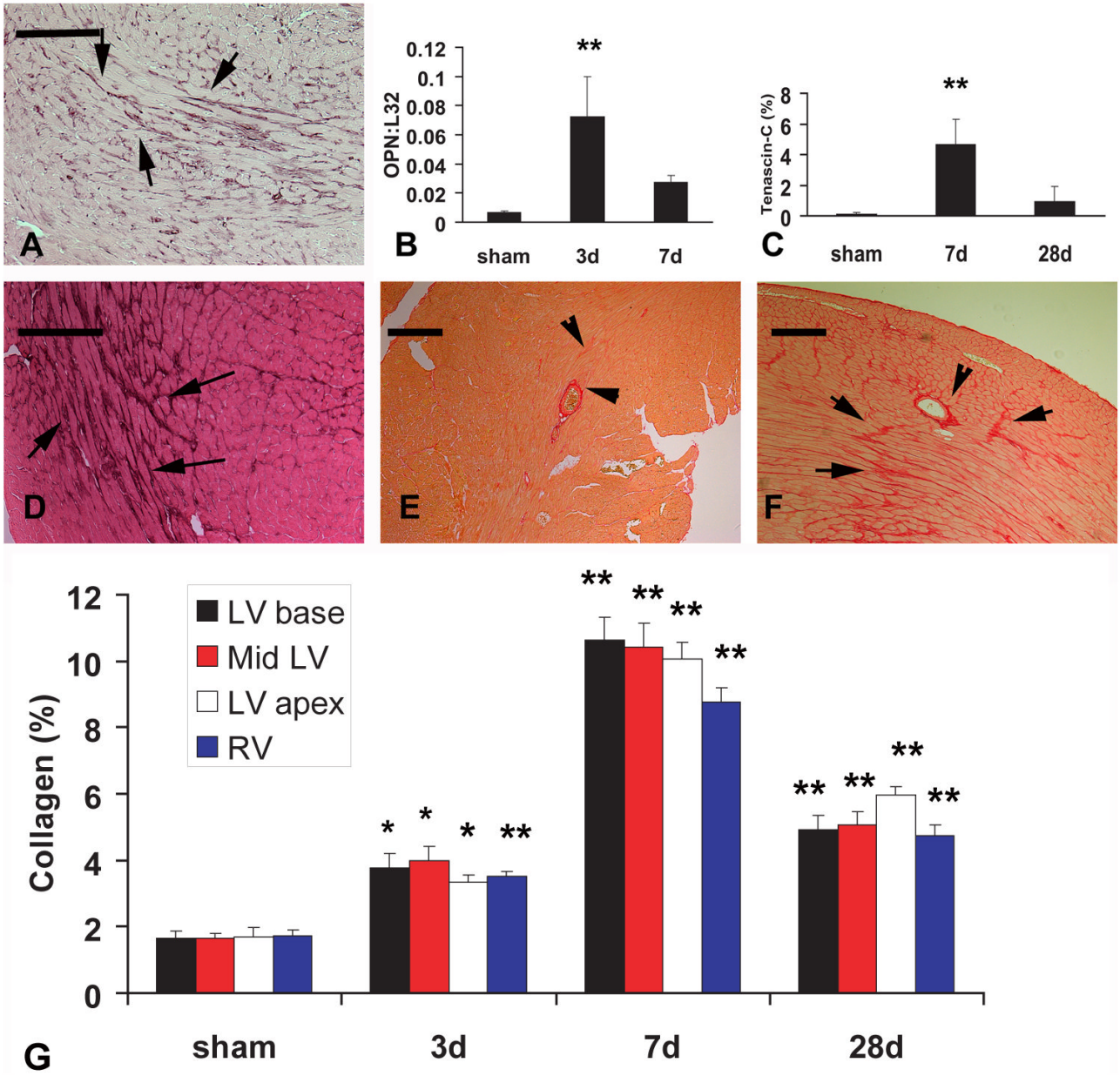

Figure 4.

Induction of matricellular proteins and collagen deposition in the pressure-overloaded mouse heart. α-smooth muscle actin staining identified abundant spindle-shaped myofibroblasts in the pressure-overloaded myocardium after 7 days of TAC (A- arrows). Upregulation of the matricellular proteins osteopontin (OPN) and tenascin-C was noted in the fibrotic myocardium. OPN mRNA was induced after 3 days of aortic banding (B) (**p<0.01 vs. sham). Interstitial deposition of tenascin-C, a protein that is not expressed in the normal heart but is induced in remodeling tissues, peaked after 7 days (**p<0.01 vs. sham) (C, D - arrows) of aortic banding. Sirius red staining identifies the collagen network in the interstitial and perivascular space of the normal heart (arrowheads). After 7 days of aortic banding, expansion of the collagen-stained area was noted in both interstitial (arrows) and periarteriolar areas (arrowhead). Quantitative analysis demonstrated a significant increase of the area stained for collagen in all segments of the pressure-overloaded heart, peaking after 7 days of TAC (G, *p<0.05 vs.

corresponding sham, **p<0.01 vs. corresponding sham). Symbols: LV, left ventricle; RV, Right ventricle. Scale bar=100 μm.

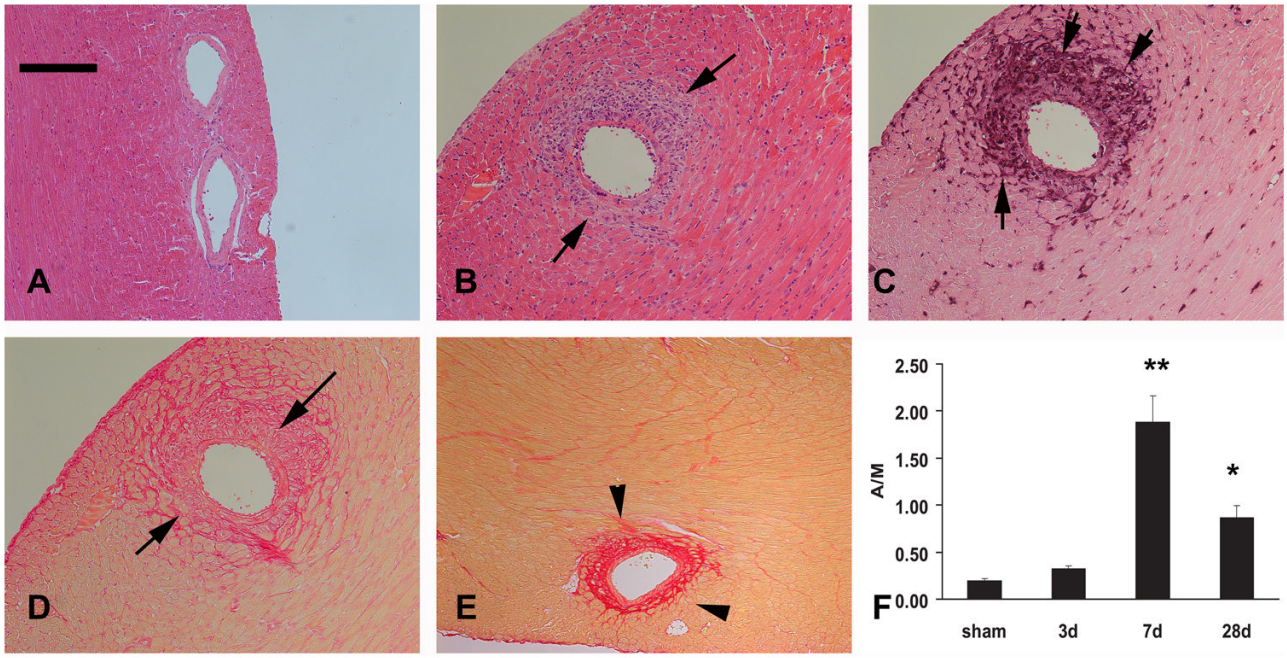

Figure 5.

Cardiac pressure overload results in development of periarteriolar inflammation and fibrosis. A: H&E staining of a normal mouse heart demonstrates that intramyocardial arterioles have a thin adventitial layer. B-D: Serial section staining of the murine myocardium after 7 days of TAC for H&E (B), Mac-2 immunohistochemistry to identify macrophages (C) and sirius red to label the collagen network (D). Expansion of the arteriolar adventitia is noted (arrows), associated with macrophage infiltration (C – arrows) and deposition of collagen (D –arrows). After 28 days of aortic banding, the fibrotic arteriolar adventitia shows deposition of dense collagen fibers (E – arrowheads). F: The ratio of the adventitial to medial arteriolar area (A:M) was used to assess the extent of adventitial expansion. The A:M area significantly increases after 7-28 days of TAC (**$p<0.01$ vs. sham; *$p<0.05$ vs. sham). Scale bar=100μm

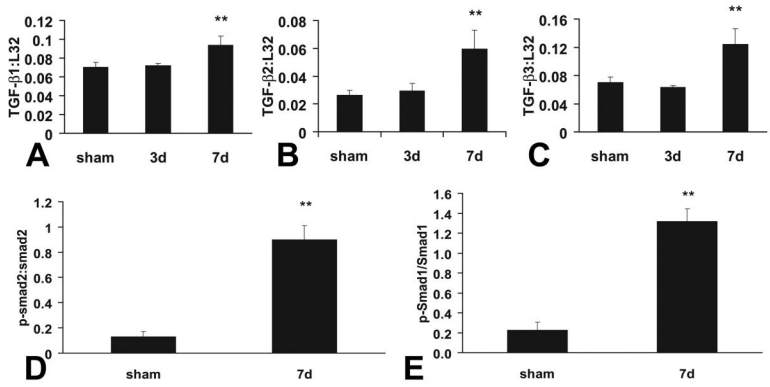

Figure 6.

Induction of TGF-β isoforms and activation of TGF-β signaling pathways in the pressure overloaded mouse heart. RPA analysis demonstrated significant TGF-β1 (A), -β2 (B) and -β3 (C) mRNA upregulation after 7 days of aortic banding. Western blotting analysis showed a marked increase in the ratio of p-Smad2:Smad2 (D) and p-Smad1:Smad1 (E) after 7 days of TAC indicating activation of the Smad2/3 and Smad1/5 pathways.

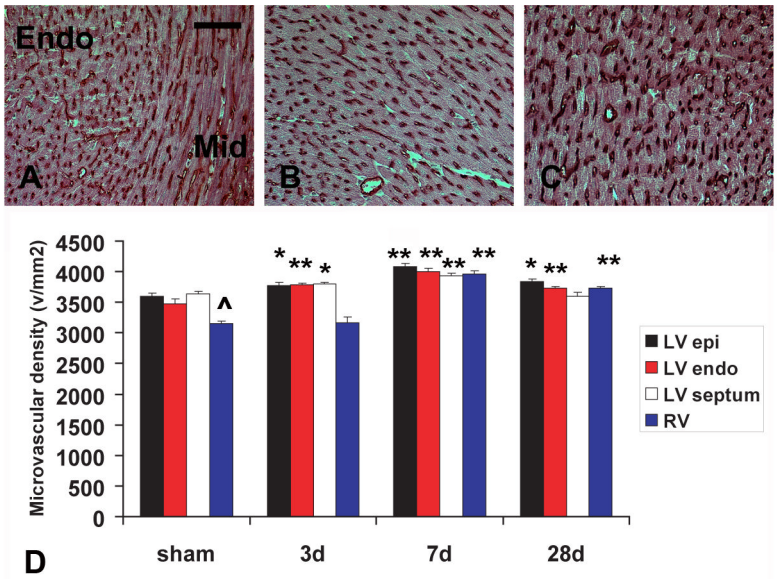

Figure 7.

Identification of microvascular endothelial cells in the pressure-overloaded myocardium using CD31 immunohistochemistry (A, sham; B, 3 days TAC; C, 28 days TAC). Quantitative analysis of microvascular density was performed in the subendocardial and subepicardial areas, where the vessels are seen in cross-section. Microvascular density significantly increased in all myocardial segments of the pressure-overloaded heart peaking after 3 days of TAC (D) (*p<0.05 vs. corresponding sham, **p<0.01 vs. corresponding sham, ˆp<0.05 vs corresponding LV epi). Symbols: LV epi, left ventricular subepicardial segment; LV endo, left ventricular subendocardial segment; RV, Right ventricle. Scale bar=60μm

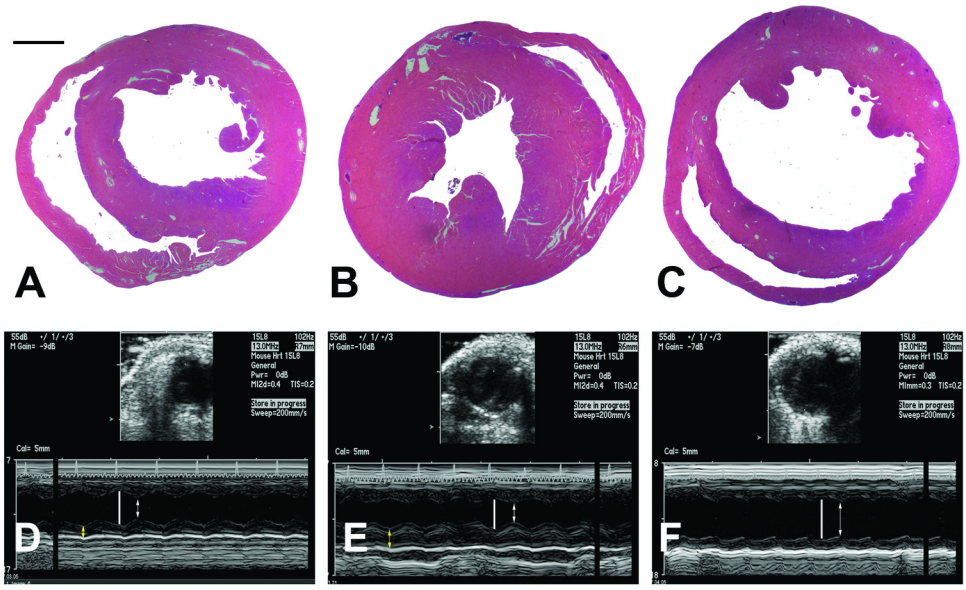

Figure 8.

Structural alterations in the pressure-overloaded mouse heart. A-C: Low magnification images of H&E-stained sections at the papillary muscle level (A, sham; B, 7 days TAC; C, 28days TAC) Scale bar=1mm. D-F M-mode echocardiographic images of the mouse heart (D, sham; E, 7 days TAC; F, 28 days TAC). Note that after 7 days of aortic banding the pressure-overloaded heart exhibits marked hypertrophy with normal chamber dimensions. LVEDD (white vertical line) and LVESD (white arrows) are comparable between sham mice (D) and animals undergoing 7 days of TAC (E). In contrast, left ventricular wall thickness (yellow arrows) is significantly increased after 7 days of banding. After 28 days of TAC significant ventricular dilation is noted accompanied by systolic dysfunction. Quantitative analysis of the echocardiographic findings is shown in Table 1.

Table 1

Echocardiographic parameters in the pressure-overloaded heart

	3d group		7d group		28d group	
	Pre	**3d**	**Pre**	**7d**	**Pre**	**28d**
LVEDD (mm)	3.58±0.2	3.30±0.12	3.52±0.08	3.28±0.09	3.46±0.15	3.66±0.23
LVESD (mm)	2.21±0.28	2.11±0.16	2.08±0.12	2.40±0.18	2.09±0.18	3.06±0.29*
FS	0.40±0.06	0.37±0.03	0.41±0.03	0.27±0.04 (p=0.08)	0.40±0.03	0.18±0.04**
LV mass (mg)	72.33±6.35	88.22±6.55	72.98±4.07**	113.55±6.34**	64.11±5.06	119.85±9.24**
IVS (mm)	0.62±0.01	0.83±0.03**	0.66±0.03	1.03±0.03**	0.60±0.03	0.88±0.03**
PW (mm)	0.63±0.02	0.79±0.05*	0.62±0.04	0.89±0.06**	0.58±0.02	0.90±0.07**

*p<0.05 vs. corresponding pre,

**p<0.01 vs. corresponding pre; values expressed as mean±SE.

Abbreviations: LVEDD (Left ventricular end-diastolic volume), LVESD (left ventricular end-systolic volume, FS (fractional shortening), LV mass (Left ventricular mass, IVS (interventricular septum thickness), PW (posterior wall thickness).